Fujiwara et al., http://www.jgp.org/cgi/content/full/jgp.201311082/DC1

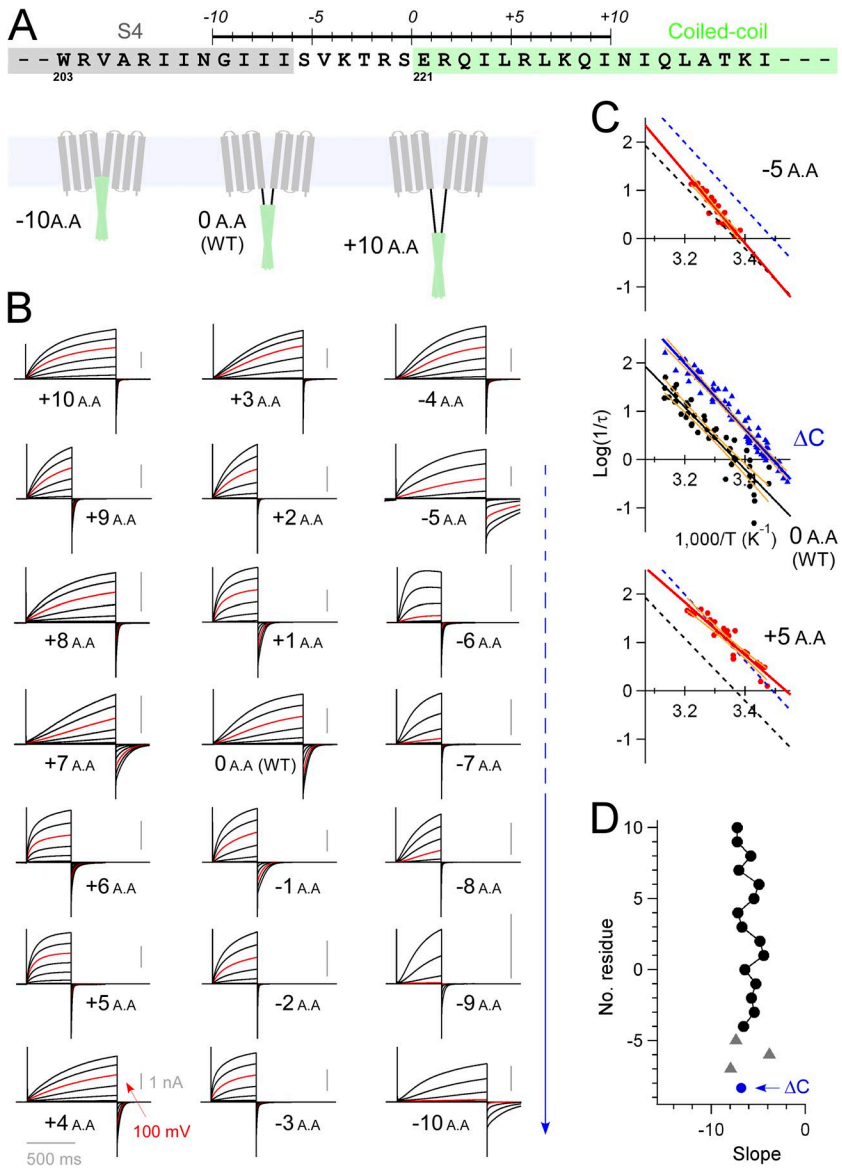

Figure S1. Electrophysiological analysis of the linker mutants. (A) Amino acid sequence of the linker mutants. (B) Representative current traces of the linker mutants at 25°C. In the recordings step, pulses were applied in 20-mV increments. Current traces recorded at 100 mV are highlighted (red traces), and scales are indicated in the +4-A.A. mutant. Thresholds of the activation were gradually shifted by reduction of the linker length (greater than or equal to −5 A.A.; blue arrow on the right side). (C) Representative correlation of the activation kinetics at 100 mV with temperature. The data of the −5-A.A. mutant were analyzed at 120 mV because of the shift of the threshold. Accumulated data and the linear regression lines with error valiance (orange line) are indicated. Mutations shifted the activation kinetics (Log (1/τ)) without significant changes of the temperature dependence (slope). WT (blue) showed the slow activation, and the C-terminal deletion (Fujiwara et al. 2012. *Nat. Commun.* 3:816; Fujiwara et al. 2013. *J. Physiol.* 591:627–640). (ΔC; monomeric channel, black) showed the fast activation, which are derived from the difference of the cooperativity of the gating. Variations of the activation kinetics (shifts of the regression lines) among the linker mutant channels were analyzed in Fig. 1 (C and D). (D) The slopes of the correlation for the activation kinetics and temperature in C are summarized for each mutant, indicating that the temperature dependence did not change significantly by mutation. The slope from the ΔC mutant is also indicated.

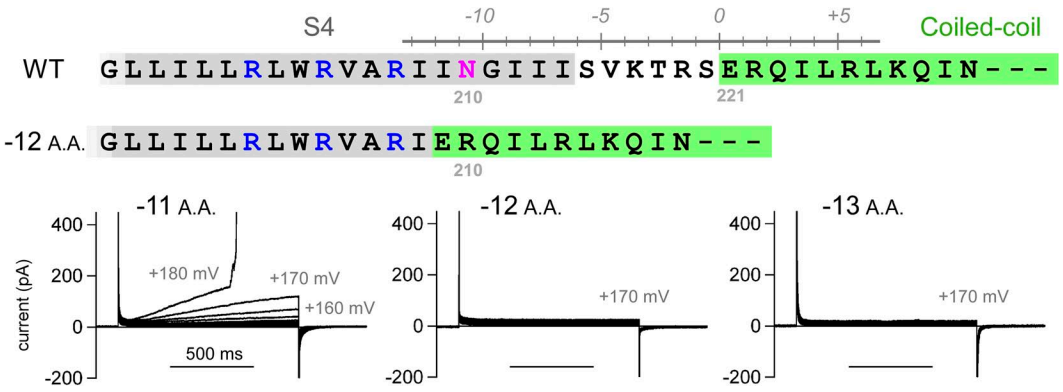

Figure S2. Intrusion of the coiled-coil domain into transmembrane region. (Top) Amino acid sequence of S4, the linker region and the coiled-coil domain (top). Voltage-sensor Arg (R201, R204, and R207) and N210 are highlighted (Tombola et al. 2008. *Neuron.* 58:546–556; Gonzalez et al. 2013. *J. Gen. Physiol.*141:275–285). Core of the S4 voltage-sensor sequence is disturbed in the −12-A.A. mutant (bottom). (Bottom) Representative current traces of the mutants at 25°C. Note that the −15- and −18-A.A. mutants also did not show functional current (not depicted). Intrusion of the coiled-coil domain into the core of the S4 voltage sensor might disrupt the channel gating, in addition to the interpretation of the restriction of the S4 movement by the coiled-coil (as discussed in the main text).

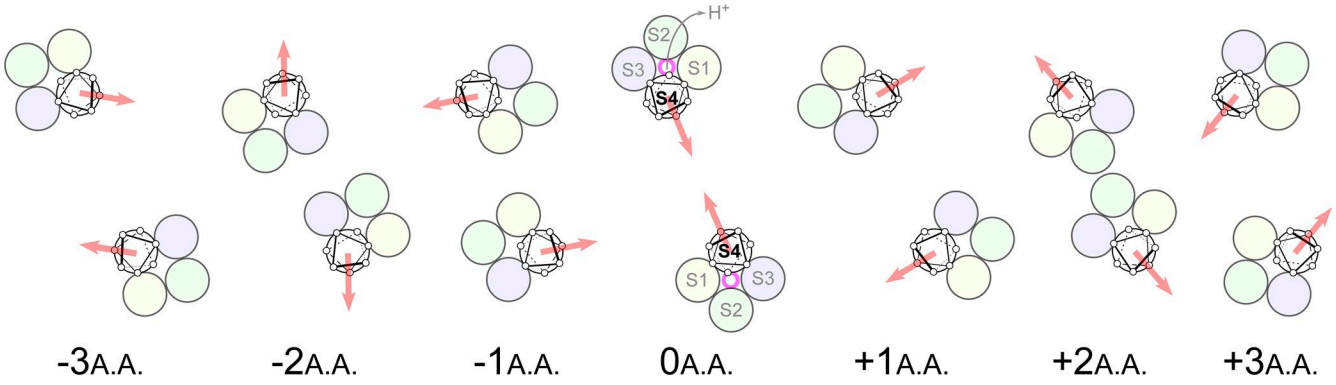

Figure S3. Conceptual illustration for the linker mutants. A pair of VSDs in each mutant viewed from the extracellular side. A shift by one residue could rotate the VSD with 100°, on the condition that a pair of VSDs connect to the coiled-coil domain with rigid structures, i.e., continuous α helices. Intervals, contacts, or directions between two S4 helices were varied by the linker length. Note that this is only a conceptual picture for illustrative purposes, and conformation of the linker domain or VSD has the potential to collapse in individual mutants.

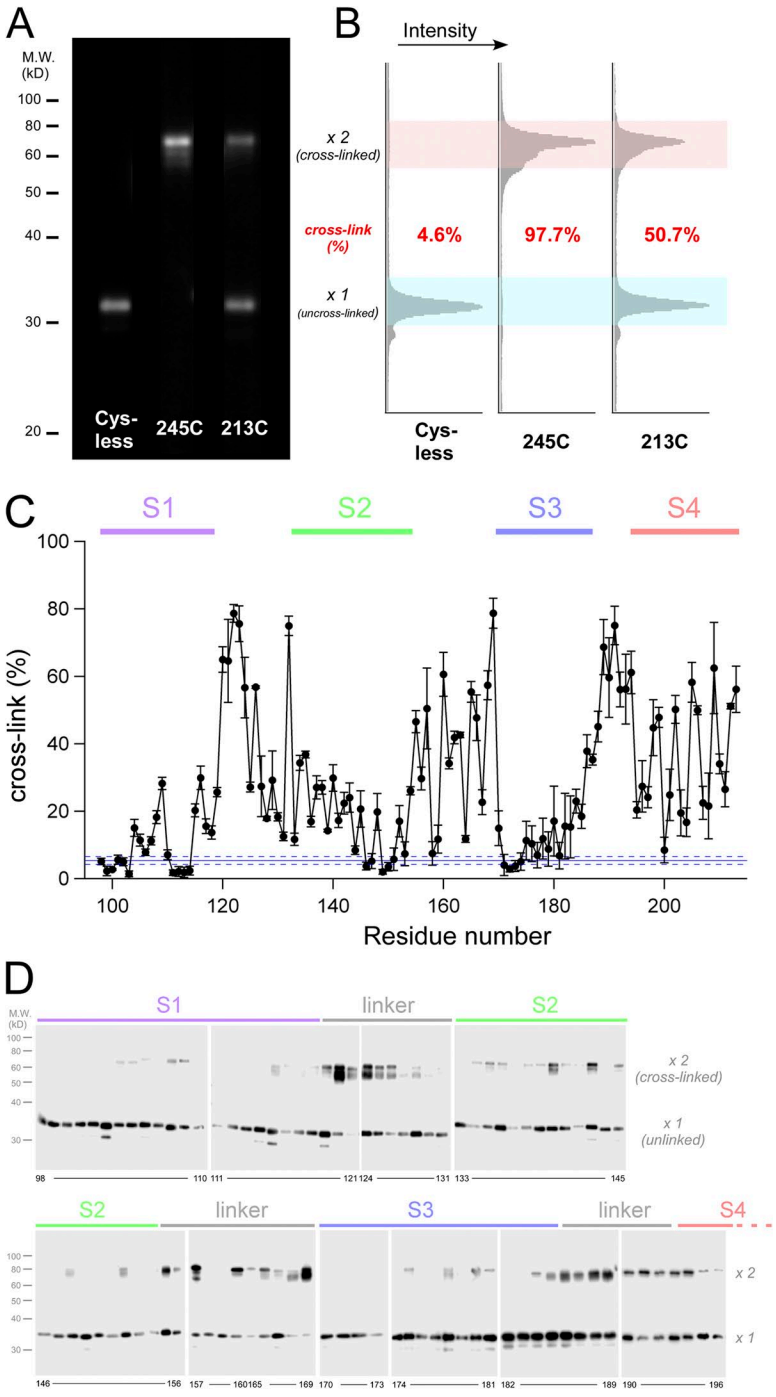

Figure S4. Analyses and data processing in the cross-linking Western blot. (A) A representative gel image for the Cys-less (C103S and C245S) 245C and 213C mutants. (B) Measurement of the band intensities and calculation of the cross-linking ratio. An intensity of 4.6% was detected in the Cys-less mutant, which is from the background signal of this assay. The average background ratio was 5.37 ± 1.19% ($n = 4$; $rR_{cysless} = 1.93$), which is indicated by the blue dotted line in C (also in Figs. 3 C, 4 D, and 5 D). We note that the cross-linking ratio of C245 is almost 100%, which is distinctly higher than those of other mutants. (C) The accumulated data of the cross-linking analyses (residues 98–212). The data were plotted as the mean ± SEM ($n = 3$ at least). The positions of the transmembrane segments (S1–S4) are indicated (top). We note that no clear periodicity was observed outside the S4 segment. (D) A representative image of the Western blot analysis for the transmembrane S1–S3 segments shown as in Fig. 3 B.

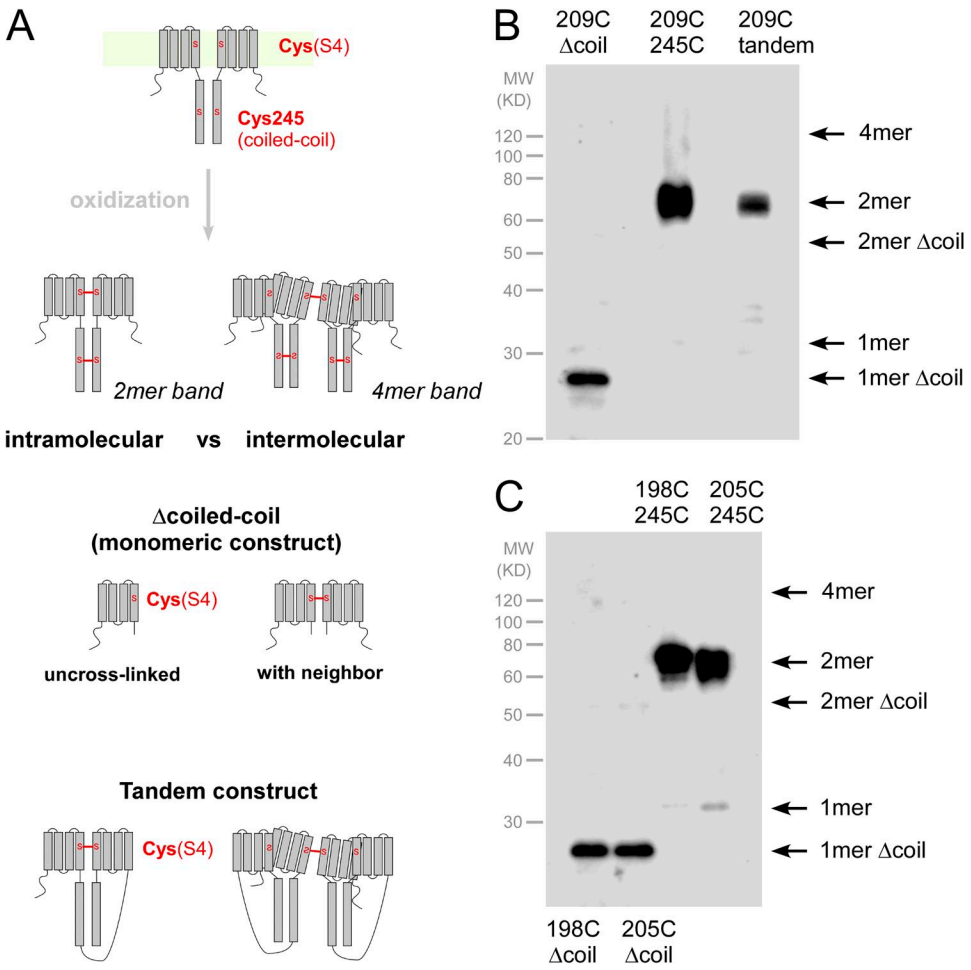

Figure S5. Intramolecular versus intermolecular cross-links. Channel constructs were designed to examine whether the cross-links between two S4 helices occur intra-molecularly or inter-molecularly. (A) Experimental strategy of the cross-linking assay. By introducing Cys into the coiled-coil assembly interface (C245), two types of cross-linking were separable (top). If cross-links between the two S4 helices are made inter-molecularly, four times the molecular weight of the cross-linking bands will be observed on the gel (top). The mutants, the coiled-coil domains of which are deleted (the monomeric Δcoil constructs), were used as the negative control (middle). Cross-links for the tandem construct were also used for the estimation (bottom). (B) A representative image of the Western blot analysis for the 209C mutants. Cys introduced at the 209 position did not form a disulfide bond in the Δcoil mutant (left). Cys at 245 in the coiled-coil region forms an intramolecular disulfide bond (Fujiwara et al. 2013. *J. Biol. Chem.* 288:17968–17975), showing a molecular band at twice the molecular weight (Fig. S4 A), which also indicated that the channel constructs were fully oxidized under the experimental condition. Four times the weight of the cross-linking band was not detected by oxidation (middle); also, that of the tandem construct was not observed (right). These results suggest that the cross-links between S4 occur intra-molecularly. (C) A representative image of the Western blot analysis for the 198C and the 205C mutants. As shown in the 209C mutants (B), no intermolecular cross-link was observed. All positions of 198, 205, and 209 are situated in the S4 segment.

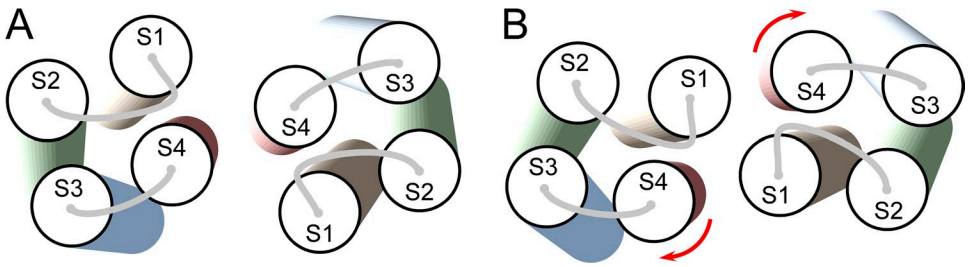

Figure S6. Two different models of the Hv dimer based on cross-linking analysis. The models depict the helix orientations viewed from the extracellular side. (A) A model based on the high cross-linking ratio between the two S4 helices, which is identical to the model in Fig. 6 B. (B) A model built with a 30° rotation of VSDs to the central axis applied to the model in A. In this model, the S1–S4 domains have rotational rearrangements by the movement of the S4 helix from the downstate to the upstate with rotation. In addition, the voltage-sensor paddle, S4 and S3b, might be able to move outside, and the four helices might be able to be tilted with a larger angle (not included in the illustration). Several studies have reported that the S4 helix moves with a certain degree of rotation during the channel gating (Cha et al. 1999. *Nature.* 402:809–813; Glauner et al. 1999. *Nature.* 402:813–817; Chakrapani et al. 2008. *Structure.* 16:398–409; Jensen et al. 2012. *Science.* 336:229–233). Small rotations can make S1 helices close to each other, which can explain the potential cross-linking of the extracellular side of S1 (Lee et al. 2008. *Proc. Natl. Acad. Sci. USA.* 105:7692–7695).